The cosmic-ray positron energy spectrum measured by PAMELA

O. Adriani,[1,2] G. C. Barbarino,[3,4] G. A. Bazilevskaya,[5] R. Bellotti,[6,7] A. Bianco,[8,9] M. Boezio,[8] E. A. Bogomolov,[10] M. Bongi,[1,2] V. Bonvicini,[8] S. Bottai,[2] A. Bruno,[6,7] F. Cafagna,[7] D. Campana,[4] R. Carbone,[8] P. Carlson,[11] M. Casolino,[12] G. Castellini,[13] C. De Donato,[12] C. De Santis,[12,14] N. De Simone,[12] V. Di Felice,[12] V. Formato,[8,9] A. M. Galper,[15] A. V. Karelin,[16] S. V. Koldashov,[16] S. A. Koldobskiy,[16] S. Y. Krutkov,[10] A. N. Kvashnin,[5] A. Leonov,[16] V. Malakhov,[16] L. Marcelli,[14] M. Martucci,[14,17] A. G. Mayorov,[16] W. Menn,[18] M. Mergé,[12,14] V. V. Mikhailov,[16] E. Mocchiutti,[8] A. Monaco,[6,7] N. Mori,[2] R. Munini,[8,9] G. Osteria,[4] F. Palma,[12,14] P. Papini,[2] M. Pearce,[11] P. Picozza,[12,14] C. Pizzolotto,[19,20,*] M. Ricci,[17] S. B. Ricciarini,[2] L. Rossetto,[11] R. Sarkar,[8] V. Scotti,[3,4] M. Simon,[18] R. Sparvoli,[12,14] P. Spillantini,[1,2] S. J. Stochaj,[8] J. C. Stockton,[8] Y. I. Stozhkov,[5] A. Vacchi,[8] E. Vannuccini,[2] G. I. Vasilyev,[10] S. A. Voronov,[16] Y. T. Yurkin,[16] G. Zampa,[8] N. Zampa,[8] and V. G. Zverev[16]

[1]*University of Florence, Department of Physics,*
I-50019 Sesto Fiorentino, Florence, Italy
[2]*INFN, Sezione di Florence, I-50019 Sesto Fiorentino, Florence, Italy*
[3]*University of Naples "Federico II",*
Department of Physics, I-80126 Naples, Italy
[4]*INFN, Sezione di Naples, I-80126 Naples, Italy*
[5]*Lebedev Physical Institute, RU-119991 Moscow, Russia*
[6]*University of Bari, Department of Physics, I-70126 Bari, Italy*
[7]*INFN, Sezione di Bari, I-70126 Bari, Italy*
[8]*INFN, Sezione di Trieste, I-34149 Trieste, Italy*
[9]*University of Trieste, Department of Physics, I-34147 Trieste, Italy*
[10]*Ioffe Physical Technical Institute, RU-194021 St. Petersburg, Russia*
[11]*KTH Royal Institute of Technology, Department of Physics,*
and the Oskar Klein Centre for Cosmoparticle Physics,
AlbaNova University Centre, SE-10691 Stockholm, Sweden
[12]*INFN, Sezione di Rome "Tor Vergata", I-00133 Rome, Italy*
[13]*IFAC, I-50019 Sesto Fiorentino, Florence, Italy*

^{14}*University of Rome "Tor Vergata",*

Department of Physics, I-00133 Rome, Italy

^{15}*National Research Nuclear University MEPhI, RU-11540 Moscow, Russia*

^{16}*National Research Nuclear University MEPhI, RU-115409 Moscow, Russia*

^{17}*INFN, Laboratori Nazionali di Frascati,*

Via Enrico Fermi 40, I-00044 Frascati, Italy

^{18}*Universität Siegen, Department of Physics, D-57068 Siegen, Germany*

^{19}*INFN, Sezione di Perugia, I-06123 Perugia, Italy*

^{20}*Agenzia Spaziale Italiana (ASI) Science Data Center, I-00044 Frascati, Italy*

(Dated: August 2, 2013)

Abstract

Precision measurements of the positron component in the cosmic radiation provide important information about the propagation of cosmic rays and the nature of particle sources in our Galaxy. The satellite-borne experiment PAMELA has been used to make a new measurement of the cosmic-ray positron flux and fraction that extends previously published measurements up to 300 GeV in kinetic energy. The combined measurements of the cosmic-ray positron energy spectrum and fraction provide a unique tool to constrain interpretation models. During the recent solar minimum activity period from July 2006 to December 2009 approximately 24500 positrons were observed. The results cannot be easily reconciled with purely secondary production and additional sources of either astrophysical or exotic origin may be required.

PACS numbers: 96.50.sb, 95.35.+d, 95.55.Vj

Cosmic-ray positrons were first observed during pioneering experiments in the sixties [1] using balloon-borne magnetic spectrometers. Positrons are a natural component of the cosmic radiation, produced in the interaction between cosmic rays and the interstellar matter. Since the first calculations of secondary positron fluxes (e.g., [2]) positrons have been shown to be extremely interesting for understanding the propagation mechanisms of cosmic rays. Furthermore, novel sources of primary cosmic-ray positrons of either astrophysical or exotic origin can also be probed.

Since July 2006, PAMELA (a Payload for Antimatter Matter Exploration and Light-nuclei Astrophysics) has been measuring the antiparticle component of the cosmic radiation. A previous PAMELA measurement of the positron fraction, the ratio of positron and electron fluxes: $\phi(e^+) / (\phi(e^+) + \phi(e^-))$, between 1.5 and 100 GeV [3, 4] showed the first clear deviation from secondary production models. Very recently, this was confirmed by the AMS collaboration that presented results on the high-energy positron fraction [5] in excellent agreement with the PAMELA data. A subsequent PAMELA measurement of the cosmic-ray antiproton energy spectrum [6] was found to be consistent with expectations from secondary production calculations. In order to explain these results both dark matter and astrophysical objects (e.g., pulsars) have been proposed as positron sources (e.g., [7]). More than 20 years ago a positron excess at high energy was postulated for the annihilation of dark matter particles in the galactic halo (e.g., [8, 9]). While extremely intriguing, such an explanation is challenged by the asymmetry between the leptonic (positrons) and hadronic (antiprotons) PAMELA data. A very high mass neutralino (e.g., [10]) is required if this is the dominant dark matter species. The allowed supersymmetric parameter space does not favour this scenario. A dark matter contribution may require pure leptonic annihilation channels (e.g., [10]) or the introduction of a new dark sector of forces (e.g., [11]). A contribution from pulsars would naturally increase the positron and electron abundances (e.g., [12]) without affecting the antiproton component. Other astrophysical models [13–15] have been proposed to explain the PAMELA positron results with an, as yet unobserved, increase in the antiproton and secondary nuclei abundances predicted at high energies ($\geq$100 GeV/n). A detailed measurement of the positron energy spectrum complements information from the positron fraction and provides stronger constraints on theoretical models than possible from the positron fraction alone.

The PAMELA experiment [7, 16] comprises (from top to bottom): a time of flight sys-

tem (TOF), a magnetic spectrometer with silicon tracker planes, an anticoincidence system (AC), an electromagnetic imaging calorimeter, a shower tail catcher scintillator and a neutron detector. These components are housed inside a pressurized container attached to the Russian Resurs-DK1 satellite, which was launched on June 15th 2006. The orbital altitude varied between 350 km and 600 km at an inclination of 70°. Data presented here were acquired over the recent solar minimum activity period from July 2006 to December 2009 (1229 days), corresponding to more than 2×10^9 triggers.

Downward-going particles were selected using the ToF information. The time-of-flight resolution of 300 ps ensured that no contamination from albedo particles remained in the selected sample. The ionization losses in the ToF scintillators and in the silicon tracker layers were used to select minimum ionizing singly charged particles. Furthermore, multiply charged tracks were rejected by requiring no spurious signals in the ToF and AC scintillators above the tracking system.

Positrons were identified by combining information from the different detector components. The misidentifications of electrons and, in particular, protons are the largest sources of background when estimating the positron signal. This can occur if the sign-of-charge is incorrectly assigned ("spillover" events) from the spectrometer data, or if electron- and proton-like interaction patterns are confused in the calorimeter data. Using strict selection criteria on the quality of the fitted tracks, the electron spillover background was estimated from flight data and simulation to be negligible below approximately 300 GeV. The proton background is much larger than the positron signal. The proton-to-positron flux ratio increases from approximately 200 at 1 GV/c to approximately 2000 at 100 GV/c. Robust positron identification is therefore required. Positron identification is based on a combination of the calorimeter shower topology and rigidity information from the tracking system. In our first publications of the positron component [3, 4] a classical analysis was employed applying strict criteria to this information. In this work the information was processed using a multivariate approach providing a significant increase in the positron selection efficiency and a cross-check of the previously published data. Specifically, the "multilayer perceptron" (MLP) network [17] type of artificial neural network [18] implemented in the TMVA [19] tool kit was used. A set of 24 classification variables was chosen in order to fully represent the topology of the shower inside the calorimeter. The analysis was performed in intervals of rigidity using events generated by a Monte Carlo simulation of the PAMELA apparatus

based on the GEANT4 code [20]. The samples of simulated electrons and protons were divided into two parts. The first part was used for the training of the multivariate algorithms while the second part was used to test the classifiers. Once the training and the testing had been performed, it was possible to classify the negatively-charged (mostly electrons) and positively-charged (protons + positrons) particles selected from the flight data.

Up to 20 GV/c, the number of electrons for each rigidity interval was obtained by fitting the output distribution for negatively-charged particles with the distribution: $p\mathcal{F}_e$, where $\mathcal{F}_e$ is the output distribution of simulated electrons and p is a normalization parameter resulting from the fit. Similarly, the number of positrons was estimated from the fit of the output distributions for positively charged particles using a mixture distribution of the neural network output for simulated electrons and protons. Figure 1 shows the neural output distributions for negatively-charged (upper panel) and for positively-charged particles (lower panel) for the rigidity interval 2.1-2.4 GV/c. A simple and high efficient event pre-selection was applied in order to have a reliable track reconstruction for energy and charge sign determination and to reduce the proton contamination by about a factor 100 requiring a shower in the calorimeter. In the bottom panel, events in the left peak of the distribution correspond to the proton residual contamination, while the peak to the right consists mostly of positron events. Excellent agreement is found between the distribution for negative events and the simulated electron distribution (solid red line in the upper panel) and between the distribution for positive events (protons and positrons) and the sum of the simulated electron and proton distributions (solid red line in the lower panel). These results were cross-checked using another multivariate classifier, "random forest" [21], a simulation with enhanced π^0 production [22] and a classical analysis [23] selecting positrons above 28 GeV. Each approach produced consistent results. At rigidities higher than 20 GV/c, positrons (and electrons) were selected by applying additional conditions based on calorimeter information to events yielding output values greater than 0.6 in Figure 1. A bootstrap procedure [24] was used to estimate the number of positrons and the positron fraction. For more details on the positron analysis see [25].

The positron energy spectrum was derived by correcting the number of positrons for selection efficiencies, live time and geometrical factor. Efficiencies were estimated directly from flight data with the exception of the track selection efficiency that was obtained from Monte Carlo simulation (e.g., see [26]). The live time was provided by an on-board clock
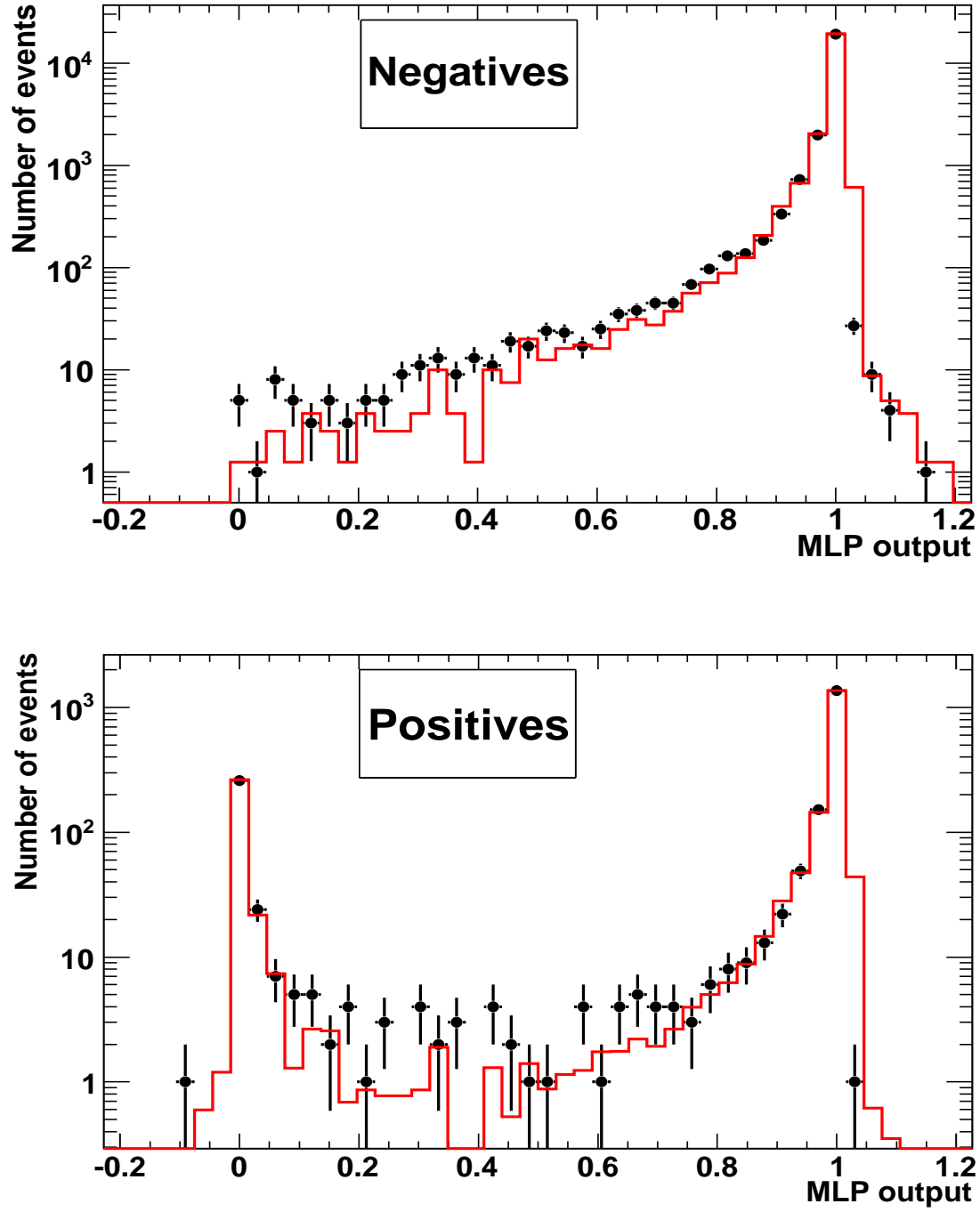
FIG. 1: The neural network output distributions for negatively-charged particles (top panel) and positively-charged particles (bottom panel) for the rigidity bin 2.1-2.4 GV/c. Top panel: distribution of simulated electrons (solid red line) superimposed on the distribution of negatively-charged particles. Bottom panel: distribution for positively-charged events (protons and positrons) fitted by the sum of the simulated electrons and protons distributions (solid red line).

that timed the periods during which the apparatus was waiting for a trigger. The geometrical factor was estimated with simulation to be constant at 19.9 cm^{2}sr in the energy range of interest. Positron energy spectra were obtained for different intervals of vertical geomagnetic cutoff, estimated in the Störmer approximation [27] using the satellite orbital information. The energy spectra were unfolded using a Bayesian unfolding procedure [28]. Spectra were combined accounting for the proper live times and using only the fluxes at energies that exceeded 1.3 times the maximum vertical geomagnetic cutoff at each cutoff interval. The total systematic uncertainty on the flux was obtained by summing in quadrature the various systematic errors due to acceptance, efficiency estimation and spectrum unfolding. A systematic uncertainty on the overall flux estimation was derived by comparing the electron energy spectra obtained using the calorimeter and the tracking information. The two sets of fluxes differed by about 5% at 2 GeV linearly increasing to 17% at 100 GeV. Thus, the total systematic uncertainty on the flux was found to vary from $\simeq 6\%$ at 2 GV to $\simeq 20\%$ above 100 GV.

The energy-binned positron data are given in Table I and in Figures 2, 3 and 4 that show the resulting positron energy spectrum [44] and positron fraction measured by PAMELA along with results from other recent cosmic-ray space- [5, 31–33] and balloon-borne [29, 30, 34–36] experiments. Between 200 GeV and 300 GeV only a lower limit at the 90% confidence level is presented because of a possible overestimation of the proton contamination in the positron sample. The positron spectrum is significantly affected by solar modulation below ~ 10 GeV. PAMELA data were acquired during a period of slowly varying solar activity, close to a solar minimum, and the fluxes are averaged over a three and a half year time period. The time dependence of the low energy positron spectrum will be the topic of a future publication. In this paper only positron data above 1.5 GeV are presented. Taking into account the experimental uncertainties and solar modulation effects, the positron fraction presented here is in agreement with the previously published PAMELA results [3, 4].

Figure 3 shows PAMELA data along with theoretical predictions. The solid line shows the original GALPROP calculation [37] (calculated using the force field approximation [38] with solar modulation parameter $\Phi = 600$ MV) assuming a pure secondary production of positrons during the propagation of cosmic rays in the Galaxy. The dotted line shows a recent calculation of secondary positrons [39] where it is argued that the progenitor proton flux is not expected to vary significantly within a few kpc from Earth and so the flux of

TABLE I: Summary of positron results. The lower limit is that for a 90% confidence level. For the flux the first and second errors represent the statistical (68% confidence level) and systematic uncertainties, respectively.

Rigidity at the spectrometer GV/c	Mean Kinetic Energy at top of payload GeV	Observed number of events e$^+$	Rescaled Flux at top of payload $(\mathrm{GeV^2 s^{-1} sr^{-1} m^{-2}}) \times 10^{-3}$	$\dfrac{\mathrm{e^+}}{(\mathrm{e^+ + e^-})}$ at top of payload
1.5 - 1.8	1.64	4644	$1762 \pm 24 \pm 111$	0.0777 ± 0.0011
1.8 - 2.1	1.94	3356	$1262 \pm 21 \pm 80$	0.0711 ± 0.0012
2.1 - 2.7	2.38	2809	$808 \pm 11 \pm 51$	0.0653 ± 0.0009
2.7 - 3.5	3.06	3755	$411 \pm 6 \pm 26$	0.0586 ± 0.0010
3.5 - 4.2	3.83	3951	$226 \pm 5 \pm 15$	0.0545 ± 0.0013
4.2 - 5	4.57	1520	$137 \pm 3 \pm 9$	0.0535 ± 0.0014
5 - 6	5.46	1124	$79.9 \pm 2.2 \pm 5.0$	0.0523 ± 0.0015
6 - 8	6.88	712	$38.4 \pm 1.0 \pm 2.6$	0.0504 ± 0.0014
8 - 10	8.9	920	$17.1 \pm 0.6 \pm 1.2$	0.0520 ± 0.0019
10 - 13	11.3	491	$8.4 \pm 0.3 \pm 0.6$	0.0557 ± 0.0023
13 - 15	13.9	448	$4.82 \pm 0.27 \pm 0.40$	0.063 ± 0.004
15 - 20	17.2	307	$2.30 \pm 0.13 \pm 0.18$	0.061 ± 0.004
20 - 28	23	195	$0.92 \pm 0.07 \pm 0.08$	0.062 ± 0.005
28 - 42	33.1	114	$0.32 \pm 0.03 \pm 0.03$	0.073 ± 0.007
42 - 65	50.2	68	$0.109 \pm 0.013 \pm 0.012$	0.099 ± 0.013
65 - 100	77.5	33	$0.034 \pm 0.006 \pm 0.005$	0.121 ± 0.022
100 - 200	135	25	$0.0118 \pm 0.0026 \pm 0.0024$	0.163 ± 0.040
200 - 300			> 0.00091	> 0.107

secondary positrons can be estimated with a few tens of percent uncertainty, at most. The high energy deviation of the experimental data with respect to theoretical calculations has led to many speculations about a primary origin of positrons. For example, the dashed line shows a calculation for secondary plus a primary contribution to the positron flux resulting
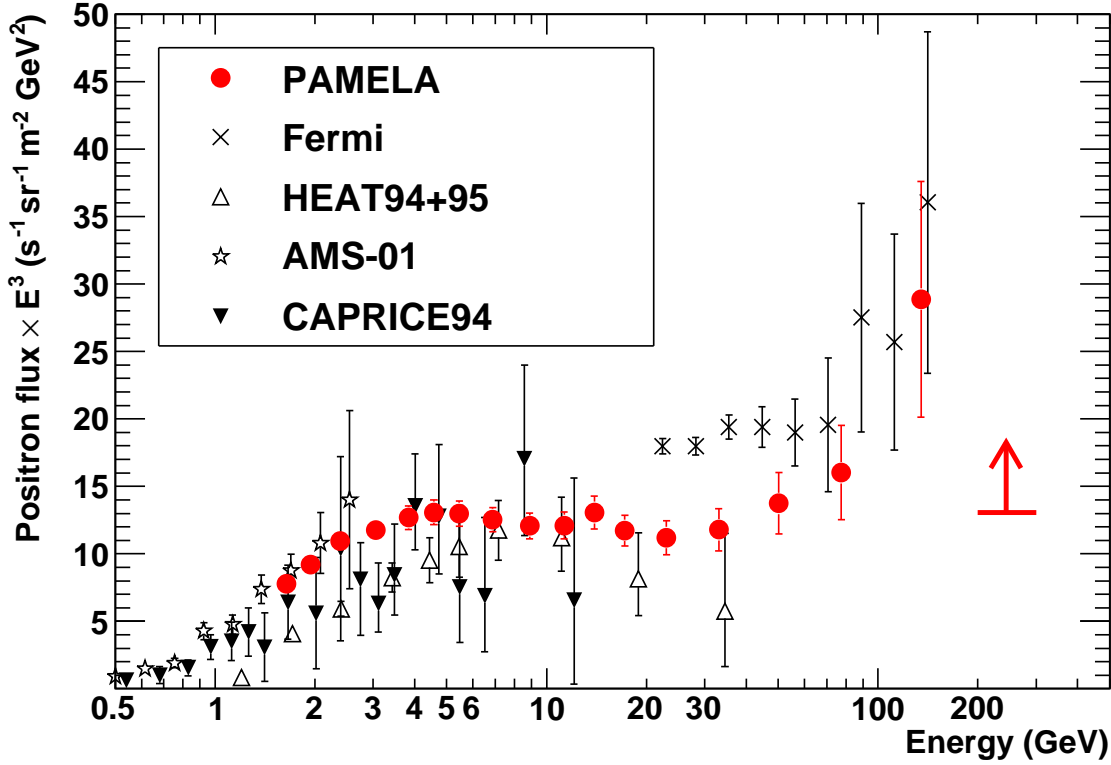
FIG. 2: PAMELA and other recent measurements of the positron energy spectrum: CAPRICE94 [29], HEAT94+95 [30], AMS-01 [31], Fermi [32]. The PAMELA, Fermi and AMS-01 results are from space-borne experiments. The PAMELA lower limit is that for a 90% confidence level. PAMELA data points include both statistical and systematic errors.

from annihilating dark matter particles of mass 1.2 TeV via a dark gauge boson of mass 580 MeV to charged lepton pairs [40].

A variety of astrophysical models have also been put forward to explain the positron excess. Pulsars are well known particle accelerators. Primary electrons are accelerated in the magnetosphere of pulsars resulting in the emission of synchrotron gamma rays. In the presence of the pulsar magnetic field, these gamma rays can produce positron and electron pairs which escape into the interstellar medium after $\sim 10^5$ years contributing to the high-energy electron and positron cosmic-ray components (e.g., [12]). As an example, in Figure 3 the dash-dotted line indicates a contribution to the secondary component from astrophysical sources such as pulsars [39]. According to [39], beyond 5-10 GeV there are
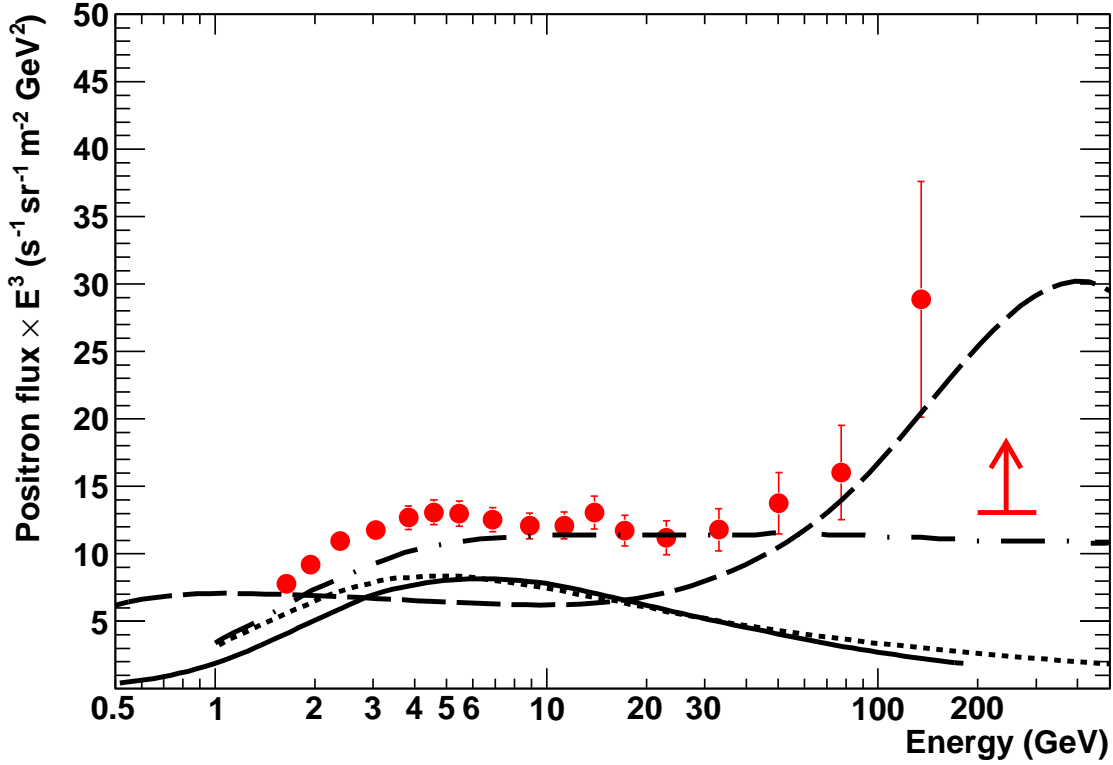
9

FIG. 3: The PAMELA positron energy spectrum data along with theoretical calculations. The PAMELA lower limit is at the 90% confidence level. PAMELA data points include both statistical and systematic errors. The solid line shows the original GALPROP calculation [37] for pure secondary production of positrons during the propagation of cosmic rays in the Galaxy. The dotted and dash-dotted lines show a recent calculation [39] for secondary and secondary plus primary (from astrophysical sources) positrons, respectively. The dashed line shows a calculation [40] for secondary plus primary positrons from dark matter annihilation.

poor constraints on the positron flux, e.g., from radio observations. It should be noted that the contribution of primaries could take any shape and that the dash-dotted line is just one possibility. Therefore, it has been concluded [39] that the positron anomaly can be explained by a few prominent astrophysical sources. Furthermore, the positron excess could also be explained [13–15] by secondary production taking place in the acceleration region of supernova remnants.

Besides the positron excess at high energies, another feature is clearly visible in the

10

positron fraction data (Figure 4). At energies below 5 GeV, PAMELA results are system-
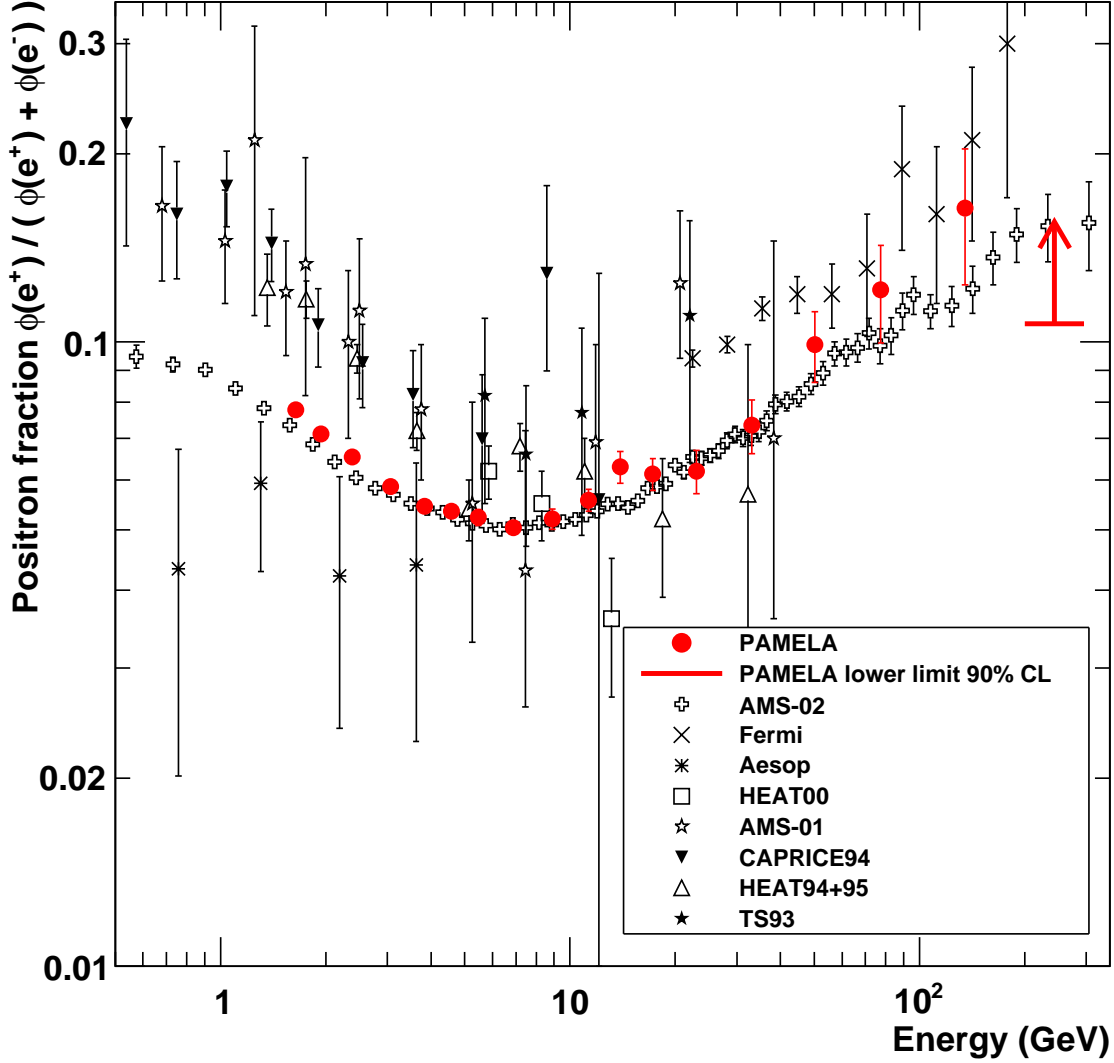

FIG. 4: PAMELA and other recent measurements of the positron fraction: TS93 [34], HEAT94+95 [35], CAPRICE94 [29], AMS-01 [31, 33], HEAT00 [41], Aesop [36], Fermi [32], AMS-02 [5]. The PAMELA, Fermi, AMS-01 and AMS-02 results are from space-borne experiments.

atically lower than other data (except AMS-02 [5] and Aesop data [36]). This low energy discrepancy with data collected during the 1990s, i.e., from the previous solar cycle that favored positively-charged particles, is interpreted as a consequence of charge-sign solar

modulation effects [42]. The AMS-02 positron fraction at low energies is, as expected, lower due to the increase in solar activity (e.g., see [43]) and shows the same high energy rise. This agreement gives good confidence that the increase of the positron flux can be ascribed to a physical effect and not to systematics affecting the measurements.

---

* Previously at INFN, Sezione di Trieste, I-34149 Trieste, Italy

[1] J. A. De Shong, R. H. Hildebrand, and P. Meyer, Phys. Rev. Lett. **12**, 3 (1964).

[2] R. J. Protheroe, Astrophys. J. **254**, 391 (1982).

[3] O. Adriani et al., Nature **458**, 607 (2009).

[4] O. Adriani et al., Astropart. Phys. **34**, 1 (2010).

[5] M. Aguilar et al., Phys. Rev. Lett. **110**, 141102 (2013).

[6] O. Adriani et al., Phys. Rev. Lett. **105**, 121101 (2010).

[7] M. Boezio et al., New J. Phys. **11**, 105023 (2009).

[8] A. J. Tylka, Phys. Rev. Lett. **63**, 840 (1989).

[9] M. Kamionkowski and M. S. Turner, Phys. Rev. D **43**, 1774 (1991).

[10] M. Cirelli, M. Kadastik, M. Raidal, and A. Strumia, Nucl. Phys. B **813**, 1 (2008).

[11] I. Cholis, G. Dobler, D. P. Finkbeiner, L. Goodenough, and N. Weiner, Phys. Rev. D **80**, 123518 (2009).

[12] A. M. Atoyan, F. A. Aharonian, and H. J. Volk, Phys. Rev. D **52**, 3265 (1995).

[13] P. Blasi, Phys. Rev. Lett. **103**, 051104 (2009).

[14] Y. Fujita, K. Kohri, R. Yamazaki, and K. Ioka, Phys. Rev. D **80**, 063003 (2009).

[15] M. Ahlers, P. Mertsch, and S. Sarkar, Phys. Rev. D **80**, 123017 (2009).

[16] P. Picozza et al., Astropart. Phys. **27**, 296 (2007).

[17] D. E. Rumelhart and J. L. McClelland, Parallel Distributed Processing: Explorations in the Microstructure of Cognition (Vol. 1) (MIT Press, 1993).

[18] R. K. Bock et al., Nucl. Instrum. Meth. A **516**, 511 (2004).

[19] TMVA documentation, http://tmva.sourceforge.net.

[20] S. Agostinelli et al., Nucl. Instrum. Meth. A **506**, 250 (2003).

[21] L. Breiman, Machine Learning **45**, 5 (2001).

[22] L. Rossetto, Ph.D. thesis, Royal Institute of Technology (KTH), Stockholm, Sweden (2012), http://pamela.roma2.infn.it/.

[23] A. Bianco, Tesi di Laurea, Università degli Studi di Trieste, Trieste, Italy (2012), http://pamela.roma2.infn.it/.

[24] B. Efron and R. J. Tibshirani, An introduction to the bootstrap method (Boca Raton, Chapman & Hall, 1993).

[25] O. Adriani et al., arXiv:1306.2198v2 (2013).

[26] O. Adriani et al., Astrophys. J. **765**, 91 (2013).

[27] N. A. of Sciences (U.S.), in Proceedings of the National Academy of Sciences of the United States of America, no. v. 17 (The Academy, 1931), URL `http://books.google.it/books?id=m20bAAAAMAAJ`.

[28] G. D'Agostini, Nucl. Instrum. Meth. A **362**, 487 (1995).

[29] M. Boezio et al., Astrophys. J. **532**, 653 (2000).

[30] M. A. DuVernois et al., Astrophys. J. **559**, 296 (2001).

[31] J. Alcaraz et al., Phys. Lett. B **484**, 10 (2000).

[32] M. Ackermann et al., Phys. Rev. Lett. **108**, 011103 (2012).

[33] M. Aguilar et al., Phys. Lett. B **670**, 103 (2008).

[34] R. L. Golden et al., Astrophys. J. **457**, L103 (1996).

[35] S. W. Barwick et al., Astrophys. J. **482**, L191 (1997).

[36] J. Clem and P. Evenson, in Proc. 30th Int. Cosmic Ray Conf. (Pune) (2007).

[37] A. W. Strong and I. V. Moskalenko, Astrophys. J. **493**, 694 (1998).

[38] L. J. Gleeson and W. I. Axford, Astrophys. J. **154**, 1011 (1968).

[39] T. Delahaye, J. Lavalle, R. Lineros, F. Donato, and N. Fornengo, Astron. Astrophys. **524**, A51 (2010).

[40] D. P. Finkbeiner, L. Goodenough, T. R. Slatyer, M. Vogelsberger, and N. Weiner, JCAP **1105**, 002 (2011).

[41] J. J. Beatty et al., Phys. Rev. Lett. **93**, 241102 (2004).

[42] M. S. Potgieter, R. A. Burger, and S. E. S. Ferreira, Space. Sci. Rev. **97**, 295 (2001).

[43] L. Maccione, Phys. Rev. Lett. **110**, 081101 (2013).

[44] The fluxes are multiplied by E^3, where E is the energy in GeV. Reducing the decades of variation of the flux, this allows for a clearer picture of the spectral shapes. However, this implies that the absolute energy uncertainties are convolved with the flux uncertainties.